Int J Earth Sci (Geol Rundsch)
DOI 10.1007/s00531-016-1405-1

ORIGINAL PAPER

Discovery of the early Jurassic Gajia mélange in the Bangong–Nujiang suture zone: Southward subduction of the Bangong–Nujiang Ocean?

Wen Lai[1] · Xiumian Hu[1] · Dicheng Zhu[2] · Wei An[3] · Anlin Ma[1]

Received: 13 April 2016 / Accepted: 21 September 2016

Abstract Mélange records a series of geological processes associated with oceanic subduction and continental collision. This paper reports for the first time the presence of Early Jurassic mélange from NW Nagqu in the southern margin of the Bangong–Nujiang suture zone, termed as the Gajia mélange. It shows typically blocks-in-matrix structure with matrix of black shale and siliceous mudstone, and several centimeters to several meters sized blocks of sandstone, silicalite, limestone and basalt. The sandstone blocks consist of homologous sandstone and two types of exotic sandstone, with different modal compositions. The Group 1 of exotic sandstone blocks consists of mainly of feldspar and quartz, whereas the Group 2 is rich in volcanic detritus. The Group 3 of homologous sandstone blocks is rich in feldspar and volcanic detritus with rare occurrence of quartz. U–Pb age data and in situ Hf isotopic compositions of detrital zircons from sandstone blocks are similar to those from the Lhasa terrane, suggesting that the sandstone blocks in the Gajia mélange most probably came from the Lhasa terrane. The YC1σ(2+) age of homologous sandstone blocks is 177 ± 2.4 Ma, suggesting an Early Jurassic depositional age for the sandstones within the Gajia mélange. The Gajia mélange likely records the southward subduction of the Bangong–Nujiang Ocean during the Early Jurassic.

Keywords Gajia mélange · Early Jurassic · Provenance analysis · Bangong–Nujiang suture zone

Introduction

The mélange is composed of the matrix, homologous blocks and exotic blocks, which are different in compositions, ages and sources (Harris et al. 1998; Hsü 1974), and is mainly formed in the tectonic setting of oceanic subduction and continental collision (e.g., Chang et al. 2001; Harris et al. 1998; Wang et al. 1988; An et al. 2016).

Wide distribution of the Jurassic ophiolite and oceanic sediments in the Bangong–Nujiang suture zone suggests that the Bangong–Nujiang Ocean did exist between the Lhasa and Qiangtang terranes (Allègre et al. 1984; Dewey et al. 1988). However, the subduction polarity remains in dispute. One traditional view is that the Bangong–Nujiang Ocean subducted northward beneath the Qiangtang terrane (Allègre et al. 1984; Chen et al. 2012; Guynn et al. 2006; Leier et al. 2007a; Yin and Harrison 2000). Alternatively, others have argued for southward subduction beneath the Lhasa terrane (Hsü et al. 1995; Kang et al. 2010; Zhu et al. 2009a, 2011b) or a double-sided subduction zone involving both northward subduction beneath the Qiangtang terrane and southward subduction beneath the Lhasa terrane (Deng et al. 2014; Hao et al. 2016; Pan et al. 2012; Zhu et al. 2013, 2016). Studying the geologic record of oceanic subduction such as mélange is fundamental to reconstruct

Electronic supplementary material The online version of this article (doi:10.1007/s00531-016-1405-1) contains supplementary material, which is available to authorized users.

✉ Xiumian Hu
huxm@nju.edu.cn

[1] State Key Laboratory of Mineral Deposits Research, School of Earth Sciences and Engineering, Nanjing University, Nanjing 210023, China

[2] State Key Laboratory of Geological Process and Mineral Resources, School of Earth Sciences and Resources, China University of Geosciences, Beijing 100083, China

[3] School of Resources and Environmental Engineering, Hefei University of Technology, Hefei 230009, China

Published online: 04 October 2016

the details of subduction process during the destruction history of the Bangong–Nujiang oceanic lithosphere.

The aim of the present study is to unravel the mélange discovered near the Gajia village in the southern margin of Bangong–Nujiang suture zone. We present detailed petrological, detrital zircon U–Pb geochronology and Hf isotope data on different types of sandstone blocks contained in the Gajia mélange of the Bangong–Nujiang suture zone in central Tibet (Fig. 1b). The results allowed us to determine the provenance and depositional age of the mélange and to demonstrate that the Bangong–Nujiang oceanic lithosphere subducted southward beneath the Lhasa terrane at the time when the Gajia mélange formed.

Geological setting

The study area is at the southern margin of Bangong–Nujiang suture zone (Fig. 1a) which continues for at least 1200 km east–west along the strike and is dominated by Jurassic deep water turbidites, mélange and ophiolite fragments (Dewey et al. 1988; Kapp et al. 2005). The Bangong-Nujiang Ocean possibly opened in the Paleozoic according the discovery of the Paleozoic ophiolite fragments (Zhu et al. 2013) and the Late Triassic turbidites unconformably on the ophiolite (Chen et al. 2005) in the suture zone, and closed during Late Jurassic–Early Cretaceous time (Baxter et al. 2009; Dewey et al. 1988; Ding et al. 2005; Zhu et al. 2016).

The Amdo terrane, located in the northeast of the Bangong–Nujiang suture zone, is dominated by Precambrian gneiss and metasedimentary rocks, Mesozoic granitoids and Cenozoic sedimentary rocks (Guynn et al. 2006; Kidd et al. 1988; Xu et al. 1985; XZBGM 1993). Guynn et al. (2012) reported bimodal distribution of Neoproterozoic (920–820 Ma) and Cambro–Ordovician (540–460 Ma) crystallization ages of the orthogeneses in Amdo terrane. Meanwhile, the Mesozoic granitoids in Amdo have bimodal distribution of 185–170 and 110–120 Ma crystallization ages, with $\varepsilon_{Hf}(t)$ values of −21.7 ~+0.6 (Liu et al. 2015; Zhu et al. 2011b).

Between the Bangong–Nujiang suture zone in the south and the Longmu–Shuanghu suture zone in the north, the southern Qiangtang terrane is mainly represented by Triassic–Jurassic shallow marine deposition, with some Later Cretaceous and Cenozoic nonmarine sedimentary rocks (XZBGM 1993). The Jurassic (150–170 Ma) acidic igneous rocks, Triassic (200–230 Ma) acidic igneous rocks, Permian (280–290 Ma) basic igneous rocks and Ordovician (450–500 Ma) acidic igneous rocks are extensively exposed on the southern Qiangtang terrane, and the $\varepsilon_{Hf}(t)$ values of the Later Triassic to Jurassic, Ordovician to Middle Triassic igneous zircons mainly range from 4.2 to 17.7, −19.4 to +2.5, respectively (Li et al. 2014b, 2015; Liu et al. 2015; Wang et al. 2015; Yang et al. 2011; Zhai et al. 2013).

To the south of the study area, the Lhasa terrane is bounded by the Indus–Yarlung Zangbo and the Bangong–Nujiang suture zones (Allègre et al. 1984; Dewey et al. 1988; Yin and Harrison 2000). The Lower Cretaceous marginal marine and deltaic clastic sediments interbedded with volcanic tuffs (Leier et al. 2007a; Zhang et al. 2012), mid-Cretaceous *Orbitolina*-bearing Langshan limestone (Rao et al. 2015; XZBGM 1993), and the Upper Cretaceous to Cenozoic nonmarine conglomerate (Kapp et al. 2005, 2007b) are extensively exposed on the northern Lhasa block. The Cretaceous magmatic rocks are also widespread on the northern Lhasa block (Zhu et al. 2009a, 2011b). The central Lhasa terrane is mainly represented by Carboniferous metasediments, Permian limestone and Jurassic siliciclastic successions (XZBGM 1993; Yin et al. 1988). And the southern Lhasa block is characterized by the Late Triassic-Early Tertiary Gangdese batholiths and Tertiary Linzizong volcanic succession (Chu et al. 2006; Ji et al. 2009; Zhu et al. 2011b) and the Cretaceous Xigaze forearc basin (An et al. 2014; Wu et al. 2010). Zhu et al. (2011a) demonstrated that the detrital zircons of Lhasa terrane define a distinctive age population of ca. 1170 Ma, which is different from both the southern Qiangtang and Amdo terrane. In addition, obviously different from the southern Qiangtang and Amdo terrane, the $\varepsilon_{Hf}(t)$ values of igneous zircons from Lhasa terrane are <2.0 in Ordovician to Middle Triassic and −5.0 to +20.0 in Middle Triassic to Jurassic (Chu et al. 2006; Dong et al. 2014; Ji et al. 2009; Zhu et al. 2009b, 2011b).

Located in the Gajia village of the Nagqu county (Fig. 1b), the Gajia mélange consists of limestone, basalt, turbidite sandstone and silicalite blocks and was considered as normal sedimentary strata in the Upper Jurassic to Lower Cretaceous (Kidd et al. 1988) or Middle Triassic (Nimaciren and Xie 2005).

Methods

The probable depositional environments and deformation characters of Gajia mélange were investigated and distinguished based on lithofacies and sedimentary features in the field. Sandstone blocks from the Gajia mélange were sampled systematically for further analysis.

Seven sandstones from the Gajia mélange were selected to do modal framework-grain analysis on thin sections. Over 350 larger than 62.5 μm grains were counted following the Gazzi–Dickinson method (Dickinson and Suczek 1979; Ingersoll et al. 1984).

Accessory minerals were separated from seven sandstone samples by elutriation and magnetic separation.

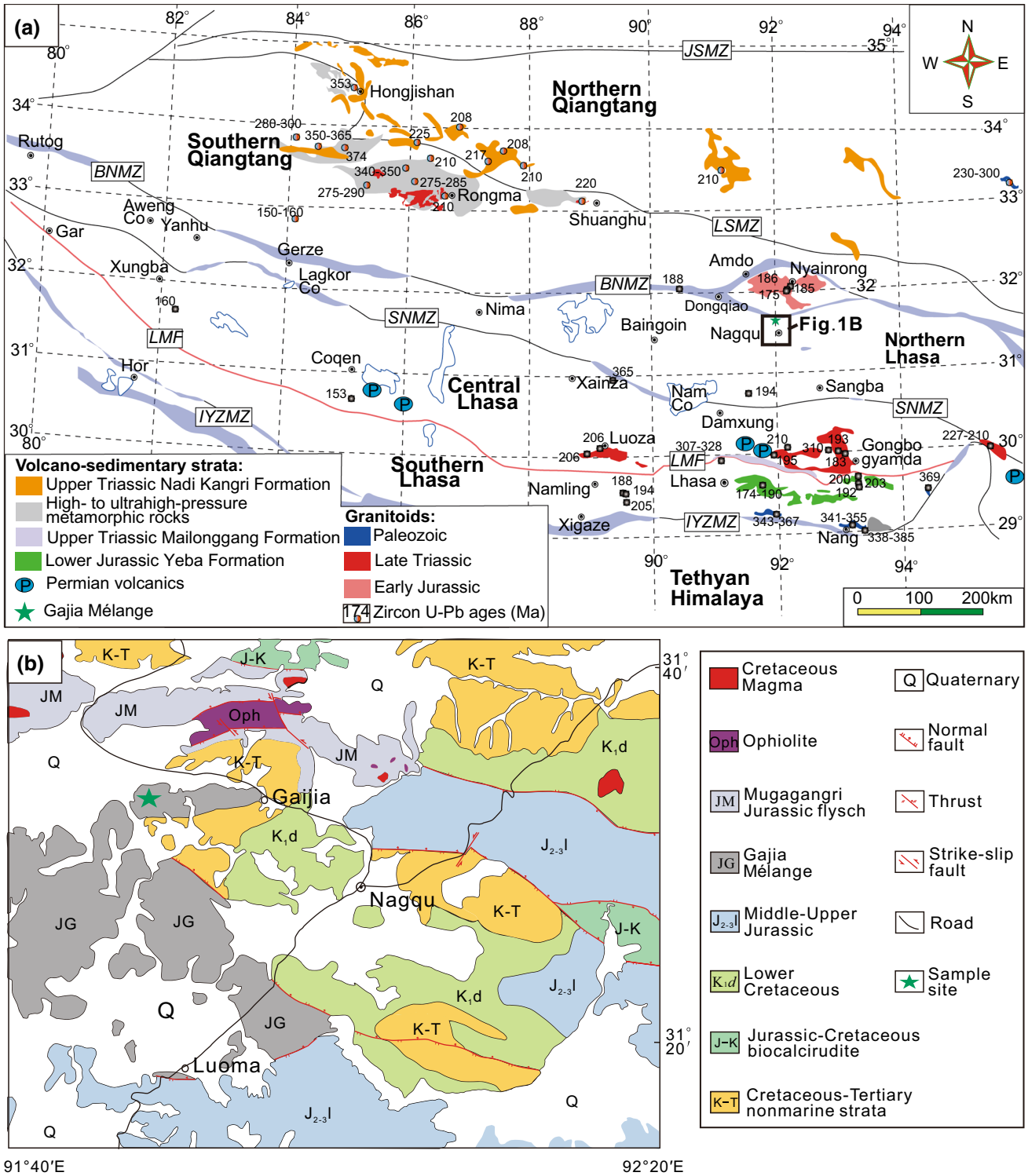

Fig. 1 **a** Simplified tectonic map of the distribution of the Mesozoic and Later Paleozoic magmatic rocks in the Lhasa terrane, Qiangtang terrane and Amdo terrane (modified from Li et al. 2014a; Zhu et al. 2013); **b** simplified geological sketch map of studying area and sampling positions (modified from Nimaciren et al. (2004)). (*LSSZ* Longmu–Shuanghu suture zone, *BNSZ* Bangong–Nujiang suture zone, *SNMZ* Shiquan River–Nam Tso Mélange zone, *LMF* Luobadui–Milashan Fault, *IYZSZ* Indus–Yarlung Zangbo suture zone)

Zircon grains were hand-picked, mounted in epoxy resin and polished. U–Pb dating of detrital zircons was conducted by LA-ICP-MS at the State Key Laboratory of Mineral Deposits Research, Nanjing University, following the method described by Jackson et al. (2004). To avoid grain-to-grain bias and treat all samples equally, the laser spot was always placed in the rim of the zircon grains and no cathodoluminescence (CL) imaging was performed. The results were calculated by GLITTER 4.4 (Van Achterbergh et al. 2001), and common Pb corrections (Andersen 2002) were conducted. The interpretation of zircon ages was based on $^{206}Pb/^{238}U$ ages for grains with ages less than 1000 Ma and on $^{207}Pb/^{206}Pb$ ages for grains older than 1000 Ma (Griffin et al. 2004). Zircon grains with discordance <10 % were accepted. Age calculations and concordia diagrams were created using Isoplot 3.23 (Ludwig 2001). The complete dataset is provided as Supplementary material.

In situ Hf isotopic analyses on detrital zircons with ages younger than 450 Ma were conducted to help constrain the likely provenance. Hf isotopic compositions were determined with a Thermo Scientific Neptune Plus MC-ICP-MS coupled to a New Wave UP 193 solid-state laser-ablation system at the State Key Laboratory for Mineral Deposits Research, Nanjing University. Zircon grains were ablated with a beam diameter of 35 μm with an 8-Hz laser repetition rate, and with energy of 15.5 J/cm^2. 1.865×10^{-11} a^{-1} for the decay constant of ^{176}Lu (Scherer et al. 2001) was applied for the calculation of the results. The $\varepsilon_{Hf}(t)$ and Hf crust model age (T^C_{DM}) were calculated, following the methodology of BouDagher-Fadel (2008) and Griffin et al. (2002), respectively. The complete dataset is provided as Supplementary material, too.

Results

The characters of the Gajia mélange in the field

Located in the south of the Dongqiao ophiolite, the Gajia mélange shows typically blocks-in-matrix structure. The black siliceous shale, mudstone and thin-bedded siltstone with broken corrugation and weakly metamorphic structure make up the "matrix." Most blocks of the Gajia mélange, with several centimeters to several meters in size, can be identified as fragments of sandstone, silicalite, limestone, basalt. Blocks in the mélange can be identified as the lenticular exotic blocks (e.g., sandstone, silicalite, limestone and basalt as shown in Fig. 2b, c) and the bedding homologous sandstone blocks (Fig. 2d).

The siliceous shaly matrix indicates that the Gajia mélange formed most probably in a bathyal-abyssal environment.

Composition of sandstone blocks

Sandstones within the Gajia mélange are mainly grain-supported, which are poorly sorted and angular-subrounded, with calcareous and ferruginous cementation. Two homologous sandstone blocks and five exotic sandstone blocks from the Gajia mélange were analyzed by the modal framework-grain analysis (Table 1; Fig. 3).

Petrographic analysis and field observations indicate that the Gajia mélange contains three distinct groups of sandstone blocks. Blocks of Group 1 and Group 2 are thick-bedded or lenticular quartzarenite, intercalated with thin-bedded siliceous mudstone (Fig. 2b, c). Blocks of Group 3 consist of turbiditic lithic-rich sandstone interbedded with mudstone in m-size outcrops. Blocks of Group 3 are bedding homologous sandstone blocks (Fig. 2d).

Group 1 lithic arkoses of exotic blocks (average composition QmFLt = 51:36:13, LmLvLs = 5:95:0, Fig. 3) consist of mainly angular to subrounded monocrystalline and feldspars (plagioclase > K-feldspar; Fig. 2e), with subordinately polycrystalline quartz, a few volcanic or rarely metamorphic lithic fragments (Fig. 3).

Group 2 consists of feldspar volcaniclastic sandstones (average composition QmFLt = 31:14:55, LmLvLs = 2:98:0) with monocrystalline and subordinately polycrystalline quartz grains, feldspars, and lithic fragments of mostly microlitic to felsitic volcanic, and minor low-rank metamorphic.

Group 3 sandstones are feldspar volcaniclastic sandstones of homologous blocks (average composition QmFLt = 20:24:56, LmLvLs = 2:98:0), dominant by subangular to rounded felsitic volcanic, feldspars (plagioclase more than K-feldspar), monocrystalline quartz grains and low-rank metamorphic lithic fragments (Fig. 2f).

Zircon, magnetite, muscovite and biotite are common accessory minerals in all three groups of sandstone blocks.

Detrital zircon U–Pb ages and Hf isotopes

Totally, 387 detrital zircons from seven sandstones of the Gajia mélange (samples shown in the Table 1) were conducted using U–Pb dating and 361 concordant ages were usable (Appendix Table S1; Fig. 4). The >80 % detrital zircons were igneous zircons with Th/U ratios over 0.4 (Belousova et al. 2002). 84 Hf isotopic analyses data with age younger than 450 Ma were acceptable (Appendix Table S2; Fig. 5).

38 of the 137 usable ages obtained from two samples of Group 1 sandstone blocks (Samples 13NQ05 and 13NQ07) are younger than 450 Ma, with a main peak at 514 Ma (Fig. 4). The youngest ages are 189 ± 4, 192 ± 3 and 195 ± 3 Ma. The complex age pattern includes clusters at 180–200, 210–250, 260–300, 310–340, 360–400, 400–530,

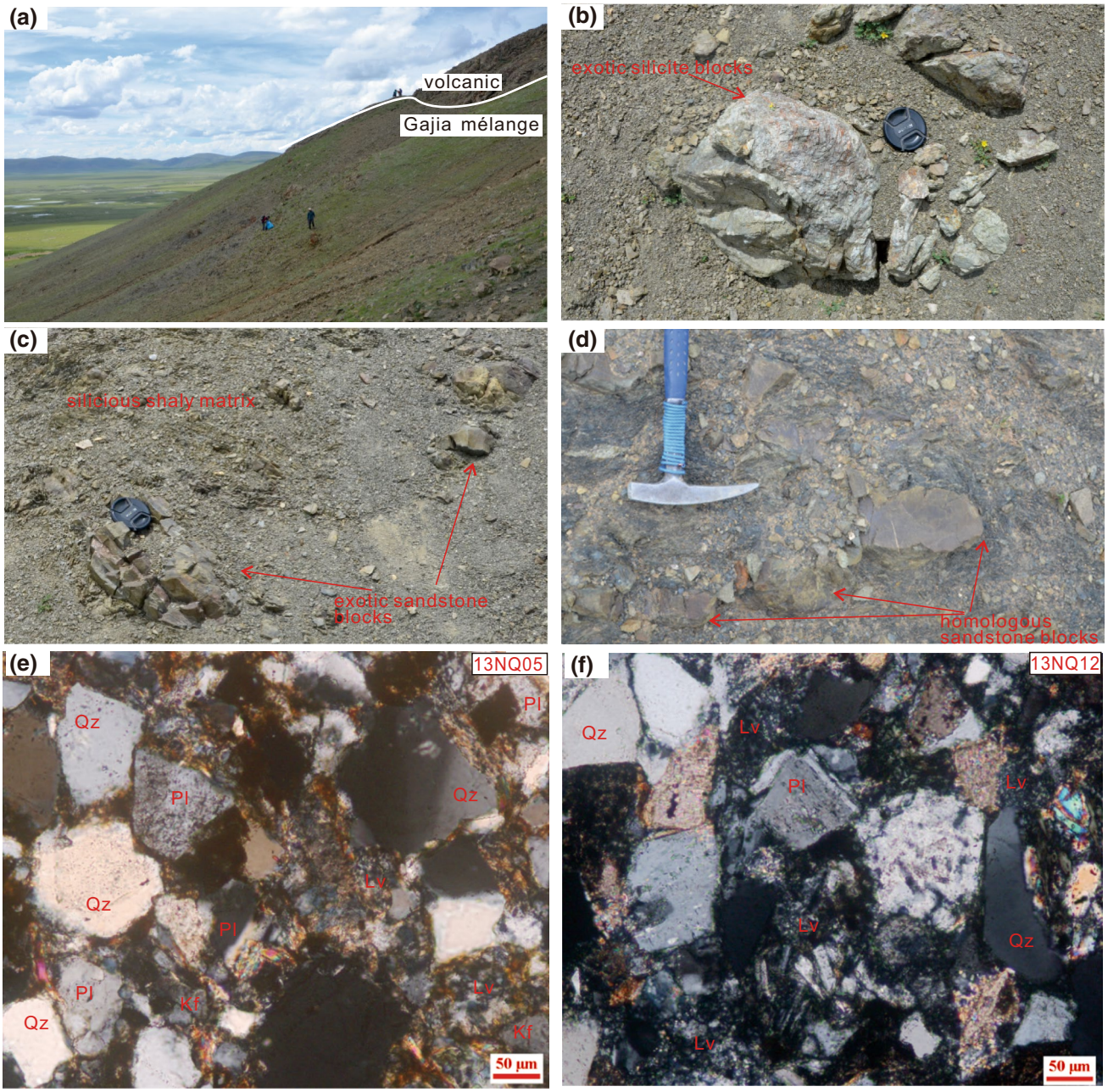

Fig. 2 Field photograph and microphotograph of sandstone blocks from the Gajia mélange. **a** Panoramic photograph for Gajia mélange, the early Cretaceous volcanic rock overlying on Gajia mélange; **b** photograph for the exotic silicalite blocks; **c** photograph for the exotic sandstone blocks with siliceous shaly matrix; **d** photograph for the homologous sandstone blocks with extensional structure; **e** feldspar sandstone (13NQ05) of exotic blocks, showing volcanic fragments and plagioclase; **f** volcaniclastic sandstone (13NQ12) of homologous blocks, showing volcanic fragments and plagioclase. (*Qz* quartz, *Pl* plagioclase, *Kf* K-feldspar, *Lv* volcanic lithic fragments)

580–700, 740–1180, 1700–2000 and 2350–2650 Ma with age peaks of ~450, ~850, ~1100, ~1850 and ~2500 Ma (Fig. 4c). 26 zircon grains of Jurassic to Silurian age show mainly negative $\varepsilon_{Hf}(t)$ (from −25.86 to +1.86) with T^{C}_{DM} model ages of 2.93–1.22 Ga (Appendix Table S2; Fig. 5).

Of the 100 concordant ages obtained from three samples of Group 2 sandstone blocks (samples 13NQ08, 13NQ10 and 13NQ11), about 22 % of zircon ages are less than 450 Ma (Fig. 4d). The youngest ages are 241 ± 4, 262 ± 4 and 263 ± 4 Ma. In addition, these samples have the clusters at 260–310, 320–360, 400–600, 700–900, 950–1200, 1700–2000, 2100–2250 and 2350–2600 Ma, with dominating peaks of ~450, ~800, ~1050, ~1850, ~2150 and ~2500 Ma. Sixteen Triassic to Silurian zircon grains show

Table 1 Sampling location and detrital composition of sandstone blocks in Gajia mélange

Group	Sample	Longitude (E)	Latitude (N)	Qm	Qp	Pl	Kf	Lv	Lm	Ls	matrix	Acc	Count
Group 1	13NQ05	91°50′03.57″	31°33′26.06″	145	5	89	44	15	1	0	82	8	389
	13NQ07	91°48′10.13″	31°33′23.28″	185	0	75	17	64	3	0	24	4	372
Group 2	13NQ08	91°48′12.23″	31°33′21.22″	147	13	40	9	235	8	0	17	2	471
	13NQ10	91°48′12.59″	31°33′20.82″	122	1	49	9	195	1	0	8	3	388
	13NQ11	91°48′13.42″	31°33′19.46″	96	1	52	10	204	4	0	15	13	395
Group 3	13NQ09	91°48′12.23″	31°33′21.22″	72	0	100	14	191	2	0	12	3	394
	13NQ12	91°48′11.45″	31°33′21.08″	70	0	58	8	214	4	0	3	2	359

Qm monocrystalline quartz, *Qp* polycrystalline quartz, *Pl* plagioclase, *Kf* K-feldspar, *Lv* total volcanic lithic grains, *Lm* total Metamorphic lithic grains, *Ls* total sedimentary lithic grains, *Acc* accessory mineral

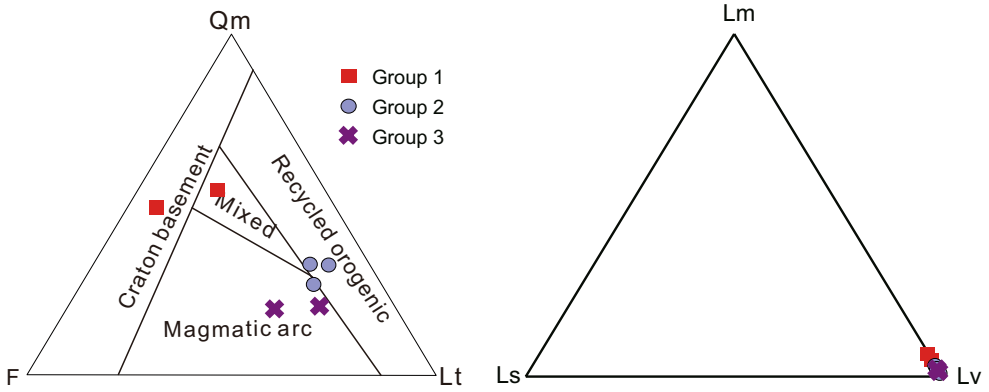

Fig. 3 Triplot of sandstone clastic compositions from the Gajia mélange. Recycled orogenic, magmatic arc and craton basement provenance fields after Dickinson et al. (1983). (*Qm* monocrystalline quartz, *F* feldspar, *Lt* total lithic grains (=Lv + Lm + Ls), *Lv* total volcanic lithic grains, *Lm* total Metamorphic lithic grains, *Ls* total sedimentary lithic grains)

$\varepsilon_{Hf}(t)$ values ranging from −12.63 to +9.14 with T^{C}_{DM} model ages of 2.15–0.76 Ga (Appendix Table S2; Fig. 5).

Among the 130 valid ages obtained from two samples of Group 3 sandstone blocks (Samples 13NQ09 and 13NQ12), 69 are younger than 450 Ma (Fig. 4e). The youngest ages are 176 ± 3, 176 ± 4, 177 ± 3 and 177 ± 3 Ma. The complex age pattern includes clusters at 170–200, 220–270, 290–330, 340–400, 400–500, 700–900, 1100–1300, 1750–2250 and 2350–2600 Ma with peaks at ~190, ~230, ~260, ~310, ~370, ~450, ~800, ~1200, ~1850 and ~2500 Ma, (Fig. 4e). Forty-two zircon grains of Jurassic to Silurian age show either positive or negative $\varepsilon_{Hf}(t)$ (from −24.03 to +11.67) with T^{C}_{DM} model ages of 2.73–0.49 Ga (Appendix Table S2; Fig. 5).

Discussion

Age constraints for the sandstone deposition within the Gajia mélange

The forming age of mélange is quite difficult to be obtained as it is not a normal sedimentary succession (Harris et al. 1998; Sun et al. 2011). According to the study of youngest U–Pb ages of detrital zircons and depositional ages known independently from biostratigraphy in the Colorado Plateau and adjacent areas, Dickinson and Gehrels (2009) suggested that the weighted mean age of youngest cluster of two or more grain ages ($n \geq 2$) overlapping in age at 1σ (YC1σ(2+)) is compatible with depositional age in 95 % with a discrepancy ≤5 Ma, for strata derived from a contemporaneously active magmatic arc. The YC1σ(2+) is testified to be compatible with biostratigraphy age and tuff age in Sangdanlin section sourced mainly from the Gangdese arc, southern Tibet (Hu et al. 2015). Thus, for mélange commonly formed in the subduction or collision zones adjacent to active magmatic arc (Harris et al. 1998; Hsü 1974), the YC1σ(2+) can provide an effective age constraint. The homologous sandstone blocks of Group 3 are rich in feldspar and volcanic clasts typically from magmatic arc (Fig. 3; Dickinson et al. 1983), indicating some of the youngest detrital zircons are from the nearby contemporary active arc.

The YC1σ(2+) age of the homologous sandstone blocks from the Gajia mélange is 177.2 ± 2.4 Ma (MSWD = 0.11)

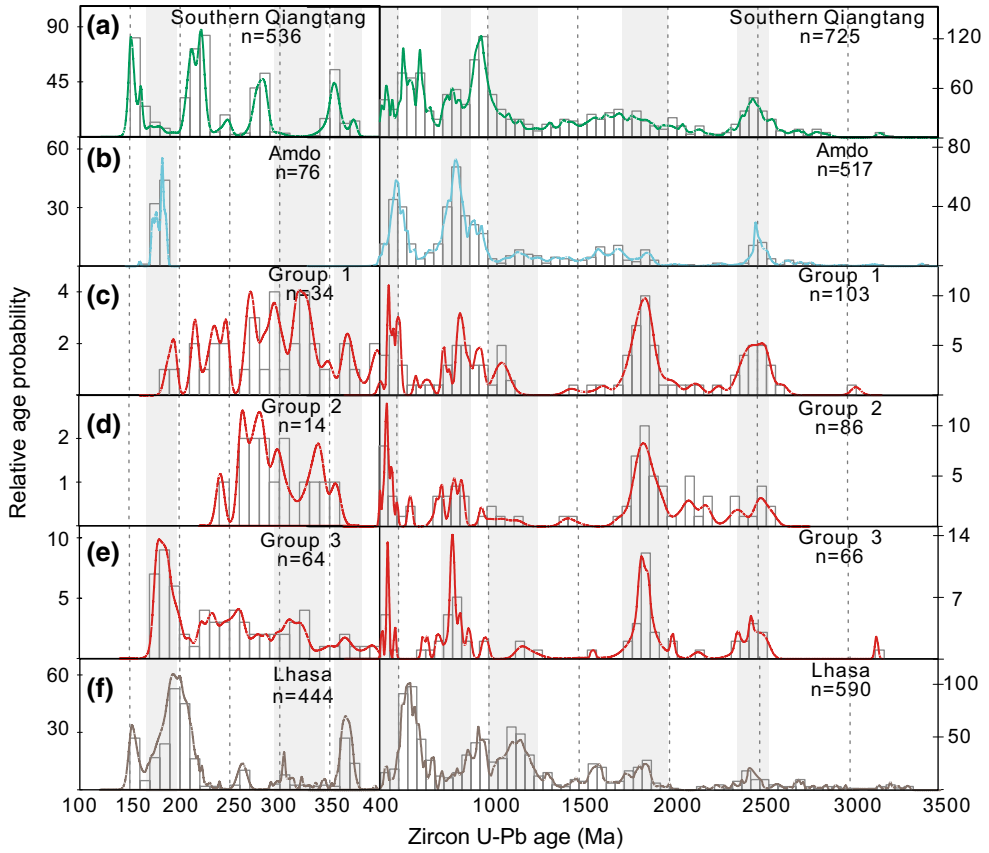

Fig. 4 Pre-Jurassic detrital zircon age distributions of Gajia mélange and relevant databases. **a** Data from the Amdo terrane (Liu et al. 2015; Zhu et al. 2011b; Guynn et al. 2012); **b** data from the southern Qiangtang terrane (Li et al. 2014b, 2015; Liu et al. 2014; Wang et al. 2015; Yang et al. 2011; Zhai et al. 2013; Dong et al. 2011; Pullen et al. 2008; Zhu et al. 2011a); **c** data from the A-type exotic sandstone blocks; **d** data from the B-type exotic sandstone blocks; **e** data from the homologous sandstone blocks; **f** data from the Lhasa terrane(Chu et al. 2006; Dong et al. 2014; Ji et al. 2009; Zhu et al. 2011a, b; Leier et al. 2007a; Zhang et al. 2012)

(Fig. 6), indicating a reasonable depositional age of Early Jurassic for the sandstones within the Gajia mélange, which means the Bangong–Nujiang oceanic subduction occurred during this time and provides an age constraint comparable to ~200–162 Ma suggested by paleomagnetic results (Yan et al. 2016).

The depositional age of the components of the Gajia mélange is also supported by the ophiolites and radiolarian cherts in the Bangong–Nujiang suture zone. The cumulate gabbros in the Bangong–Nujiang suture zone have recently been dated at 164–187 Ma from Dengqen to Dongqiao, indicating that the Bangong–Nujiang ophiolites were formed during the Early–Middle Jurassic (Wang et al. 2016). Moreover, radiolarian cherts indicate that deep-marine environment prevailed in Bangong–Nujiang Ocean during the early Middle Jurassic in Gerze (Baxter et al. 2009), the Jurassic in Dongqiao (Wang and Tang 1984), respectively.

Provenance interpretation

U–Pb age spectra and $\varepsilon_{Hf}(t)$ values of detrital zircons are collected from all available sources (including the Lhasa terrane, the southern Qiangtang terrane, and Amdo terrane) and used to constrain the likely provenance of sandstone blocks.

Detrital zircon ages range widely in different Tibetan terranes (Qiangtang, Lhasa and Himalaya) (Gehrels et al. 2011), with some important features for each unit. For example, the major Precambrian age peaks in the southern Qiangtang terrane occur at ~550, ~800, ~950 and ~2500 Ma (Fig. 4a), while the Amdo terrane with ~500, ~800 and ~2500 Ma (Fig. 4b), and the Lhasa terrane with ~550, ~950, ~1170, ~1600, ~1850 and ~2500 Ma (Fig. 4f).

In addition, the age peaks and $\varepsilon_{Hf}(t)$ values of the Silurian to Jurassic igneous zircons are also quite different among these units (as shown in Figs. 1a, 5). The Mesozoic

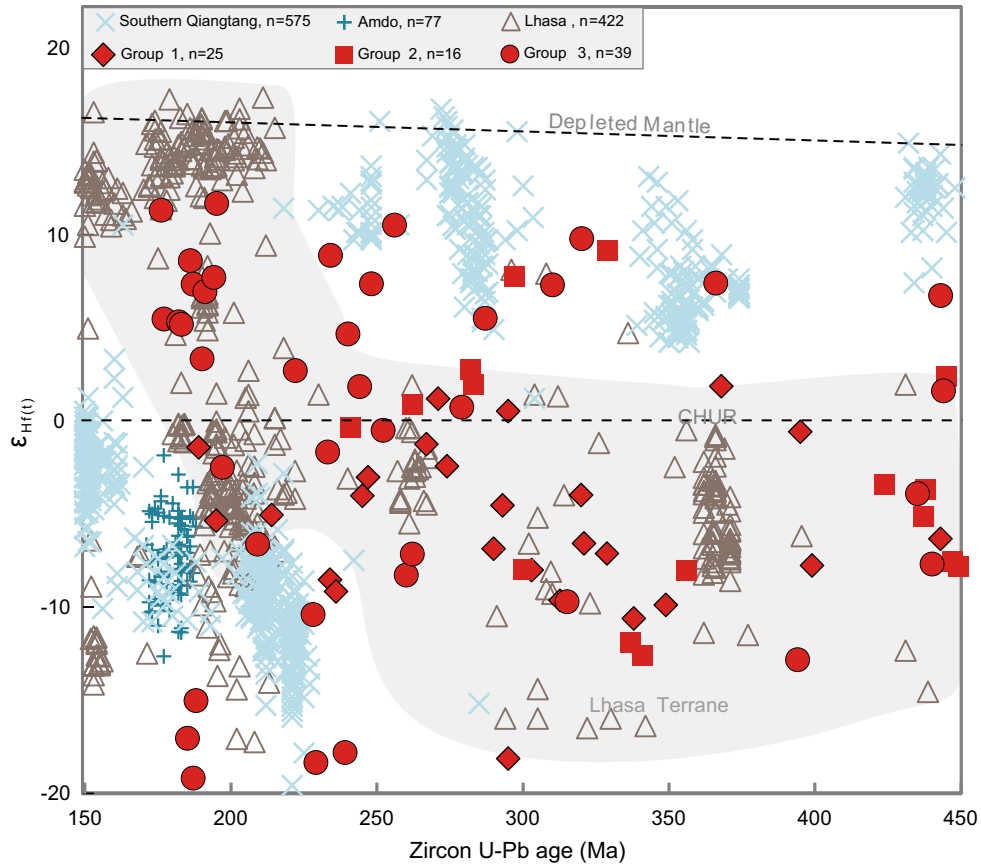

Fig. 5 Plot of U–Pb detrital ages versus $\varepsilon_{Hf}(t)$ values of the detrital zircon from the Gajia mélange and crystallized zircon from igneous rocks in southern Qiangtang terrane (Hao et al. 2016; Li et al. 2014b, 2015; Liu et al. 2014; Wang et al. 2015; Yang et al. 2011; Zhai et al. 2013), Amdo terrane (Liu et al. 2015; Zhu et al. 2011b) and Lhasa terrane (Chu et al. 2006; Dong et al. 2014; Ji et al. 2009; Zhu et al. 2011b)

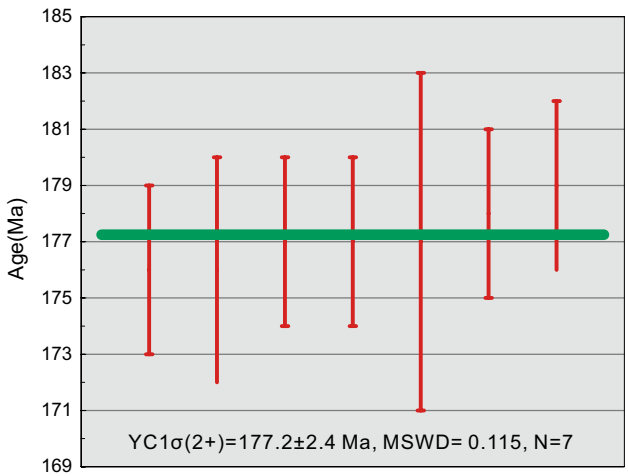

Fig. 6 Youngest U–Pb age for weighted mean ages of detrital zircon from the Gajia mélange [YC1σ(2+) age calculation after Dickinson and Gehrels (2009)]

granitoids in the Amdo have bimodal distribution of 185–170 Ma and 110–120 Ma crystallization ages, with $\varepsilon_{Hf}(t)$ values of −21.7 to +0.6 (Liu et al. 2015; Zhu et al. 2011b). The $\varepsilon_{Hf}(t)$ values of the Later Triassic to Jurassic, Ordovician to Middle Triassic igneous zircons from southern Qiangtang terrane mainly range from 4.2 to 17.7, −19.4 to +2.5, respectively (Li et al. 2014b, 2015; Liu et al. 2015; Wang et al. 2015; Yang et al. 2011; Zhai et al. 2013). The $\varepsilon_{Hf}(t)$ values of igneous zircons from Lhasa terrane are <2.0 in Ordovician to Middle Triassic and −5.0 to +20.0 in Middle Triassic to Jurassic (Chu et al. 2006; Dong et al. 2014; Ji et al. 2009; Zhu et al. 2009b, 2011b).

Lack of detrital zircons with age peaks of 200–400, ~1100 and ~1850 Ma precludes the Amdo terrane provenance as the main source for the Gajia mélange (Fig. 4).

Detrital zircons in the Group 1 with age peaks of ~450, ~850, ~1100, ~1850 and ~2500 Ma are much more comparable to those of the Lhasa terrane than to those of southern

Qiangtang terrane (Fig. 4). Moreover, The Triassic to Ordovician detrital zircons with mainly negative $\varepsilon_{Hf}(t)$ (−25.86 to +1.86) are similar to the zircons from Lhasa terrane (Chu et al. 2006; Dong et al. 2014; Ji et al. 2009; Li et al. 2014a; Zhu et al. 2009b, 2011b) rather than those from southern Qiangtang terrane (Li et al. 2014b, 2015; Liu et al. 2014; Wang et al. 2015; Yang et al. 2011; Zhai et al. 2013), as shown in Fig. 4, suggesting a possible greater contribution from the Lhasa terrane.

Ages of detrital zircons from the Group 2 exotic sandstone blocks range from 241 to 2593 Ma, with peaks ~450, ~800, ~1050, ~1850, ~2150 and ~2500 Ma. This age distribution is partly similar to the southern Qiangtang and Lhasa terranes (as shown in Fig. 4). However, 14 of the 16 Triassic to Silurian detrital zircon grains with $\varepsilon_{Hf}(t) < +2$ are similar to the Late Triassic sediments in central Lhasa terrane (Li et al. 2014a) and extremely different from the simultaneous igneous zircons in the southern Qiangtang terrane (Fig. 5), indicating the Group 2 exotic sandstone blocks are mainly from the Lhasa terrane.

Group 3 feldspar volcaniclastic sandstones of homologous blocks yield detrital zircons with the pre-Silurian age peaks at ~450, ~800, ~1200, ~1850 and ~2500 Ma, which are widespread in Lhasa sedimentary units (Leier et al. 2007b; Zhang et al. 2012, 2011a). The zircons peaks of ~190 Ma with mainly positive $\varepsilon_{Hf}(t)$ (−2.49 to +11.67), ~260 Ma with positive or negative $\varepsilon_{Hf}(t)$ (−18.34 to +5.50), ~310 and ~370 Ma with mainly negative $\varepsilon_{Hf}(t)$ (−18.34 to +1.62) may be derived from the Jurassic granite or diorite (Chu et al. 2006; Ji et al. 2009; Zhu et al. 2011b), the Permian granite (Zhu et al. 2009b) or the Late Triassic sandstones (Li et al. 2014a), the Late Triassic sandstones (Li et al. 2014a) or gneiss (Dong et al. 2014), respectively (as shown in Fig. 5). Moreover, six detrital zircons with extremely negative $\varepsilon_{Hf}(t)$ (−24.03 to −15.02) resemble the Early Jurassic granite in central Lhasa terrane reported by Zhu et al. (2011b). However, less than 30 % of the Silurian to Jurassic zircons display similar $\varepsilon_{Hf}(t)$ values to those from the southern Qiangtang terrane. In conclusion, provenance of Group 3 homologous sandstone blocks is most likely to be the Lhasa terrane rather than the southern Qiangtang terrane.

Note that the ranges of age peaks older than 400 Ma of Group 1, 2 and 3 are significant deviation from collected data of Lhasa terrane. Because the quantity of detrital zircons with different age peaks is strongly affected by grain size of sorting, times of recycling, distribution of provenance, and erosion rate. The detrital zircons older than 400 Ma in Group 1, 2 and 3 may be recycled times and only from fine sandstone while the collected detrital zircons of Lhasa terrane were from samples of different sizes in different places. Therefore, it is entirely possible that the ranges of age peaks older than 400 Ma of Group 1, 2 and 3 deviate from collected data of Lhasa terrane. Based on integrated research of the strata (Leier et al. 2007a; Yin et al. 1988; Zhang et al. 2004), magmatism (Liu et al. 2014; Zhu et al. 2013, 2016), ophiolite (Fan et al. 2014) and paleontology (Baxter et al. 2009) in Bangong–Nujiang suture zone and adjacent area, the Bangong–Nujiang Ocean last to the Late Jurassic to Early Cretaceous. The Gajia mélange with YC1σ(2+) age of ~177 Ma was formed far before the onset of the Lhasa-Qiangtang collision. Besides, accommodated >230 km of shortening (>55 %) in the Lhasa region (Kapp et al. 2007a), the Gajia area was ~400–500 km away from the Jurassic-Paleozoic magma zone on Lhasa terrane (as shown in Fig. 1a) during the Early Jurassic, which is much shorter than the 600–800 km distance between Okinawa Trough and its present source area, southeast China (Diekmann et al. 2008; Dou et al. 2012).

Group 1, 2, and 3 sandstones were thus most possibly sourced from the Lhasa and deposited near or on the northern marginal of Lhasa before the Lhasa-Qiangtang collision onset. During the Early Jurassic, clastics from the southern Qiangtang terrane or Amdo terrane to the north of the Bangong–Nujiang Ocean seemed impossible to bypass the Bangong–Nujiang oceanic basin and deposit in the Gajia area.

Tectonic model for the Gajia Mélange

The extensive presence of Late Mesozoic(164–102 Ma) magmatic rocks in central–northern Lhasa subterrane has been attributed to the southward subduction of the Bangong–Nujiang Ocean (e.g., Pan et al. 2006; Zhu et al. 2009a, b). A slab break-off model has also been suggested to explain a magmatic flare-up with an increased mantle contribution at 110 ± 3 Ma in Xainza of the central and northern Lhasa subterrane (Chen et al. 2014). If the Bangong–Nujiang Ocean closed only by northern subduction (Allègre et al. 1984; Chen et al. 2012; Guynn et al. 2006; Kang et al. 2010; Leier et al. 2007a; Yin and Harrison 2000), it is difficult for a slab break-off model to account for contemporary magmatic flare-ups in central–northern Lhasa sub-blocks during the Early Cretaceous and hard to explain the double mélange belts located in both north and south of the Early–Middle Jurassic ophiolite, as observed. As discussed above, southern subduction of the Bangong–Nujiang Ocean seems to also exist (Deng et al. 2014; Hao et al. 2016; Pan et al. 2012; Zhu et al. 2013, 2016).

Located in the south of the Early Jurassic Dongqiao ophiolite, the Gajia mélange was formed as the southern subduction complex not the collision production for the clastics of the Gajia mélange was only sourced from the Lhasa terrane and deposited in a bathyal-abyssal environment on the north margin of the Lhasa terrane. During the Early Jurassic subduction beneath the Lhasa terrane

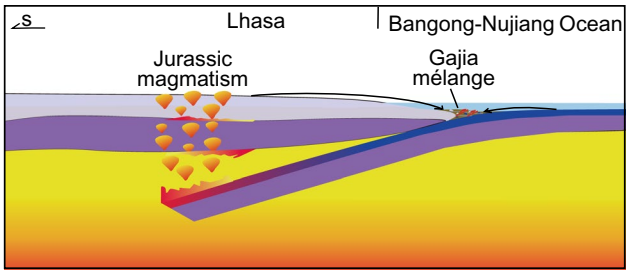

Fig. 7 Simplified tectonic model for the Gajia mélange

(Fig. 7), shed from the Lhasa terrane of the active margin, Group 1 lithic arkoses and Group 2 feldspar volcaniclastic sandstones of exotic blocks were laid in the trench and/or in a trench-slope basin on top of the subduction complex. At the same time, sediments from the Lhasa terrane, magma arc and oceanic crust deposited in the trench as the "matrix," and the sandstone beds in the "matrix" turned into Group 3 homologous sandstone blocks broken or boudinaged by tectonic deformation during continuing subduction of the Bangong–Nujiang Ocean.

About at the same time, abyssal sediments together with seamounts lying on Bangong–Nujiang Oceanic crust were offscraped and accreted into the growing subduction complex as exotic blocks of chert, limestone and basalt. The Gajia mélange provides additional sedimentary evidence for this southward subduction and locates the southward subduction zone.

Conclusions

Based on the field evidence and provenance analysis of sandstone blocks from the Gajia mélange of the Bangong–Nujiang suture zone, we can conclude that:

1. Showing typically blocks-in-matrix structure with black shale and mudstone as "matrix," the Gajia mélange was identified as mélange rather than normal sedimentary strata as mapped before, deposited in the bathyal-abyssal environment during the Early Jurassic (ca. 177 Ma).
2. According to field evidence, petrology, detrital zircon age pattern, and Hf isotope values, the sandstone blocks in the Gajia mélange can be divided into three groups: Group 1, the lenticular exotic sandstone blocks are rich in feldspar and quartz and lack of volcanic debris, with ~25 % Late Paleozoic and Mesozoic detrital zircon. Group 2, the lenticular exotic sandstone blocks are rich in volcanic debris and lack of feldspar and quartz, with ~14 % Late Paleozoic and Mesozoic detrital zircon. Group 3, the bedding homologous sandstone blocks are rich in feldspar and volcanic debris and lack of quartz, with ~50 % Late Paleozoic and Mesozoic detrital zircon.
3. Detrital zircon U–Pb ages and Hf isotopes data suggest the sandstone blocks were mostly derived from the Lhasa terrane, indicated that the Gajia mélange in Nagqu of the Early Jurassic southward subduction of Bangong–Nujiang suture zone records the Bangong Ocean beneath the Lhasa terrane.

Acknowledgments This work benefited from discussions with Jiangang Wang and Zhong Han. We thank Bin Wu, Xiong Yan for their assistance in the laboratory and Dehua Zhang for their help in the field. This study was financially supported by the CAS Strategic Priority Research Program (B) (XDB03010000) and the Chinese NSFC Project (41472081).

References

Allègre CJ, Courtillot V, Tapponnier P, Hirn A, Mattauer M, Coulon C, Jaeger JJ, Achache J, Scharer U, Marcoux J, Burg JP, Girardeau J, Armijo R, Gariepy C, Gopel C, Li T, Xiao X, Chang C, Li G, Wang N, Chen G, Han T, Wang X, Den W, Sheng H, Cao Y, Zhou J, Qiu H, Bao P, Wang S, Wang B, Zhou Y, Xu R (1984) Structure and evolution of the Himalaya–Tibet orogenic belt. Nature 307:17–22. doi:10.1038/307017a0

An W, Hu X, Garzanti E, BouDagher-Fadel MK, Wang J, Sun G (2014) Xigaze forearc basin revisited (South Tibet): provenance changes and origin of the Xigaze Ophiolite. Geol Soc Am Bull 126:1595–1613. doi:10.1130/b31020.1

An W, Hu X, Garzanti E (2016) Sandstone provenance and tectonic evolution of the Xiukang Mélange from Neotethyan subduction to India–Asia collision (Yarlung–Zangbo suture, south Tibet). Gondwana Res. doi:10.1016/j.gr.2015.08.010

Andersen T (2002) Correction of common lead in U–Pb analyses that do not report ^{204}Pb. Chem Geol 192:59–79

Baxter AT, Aitchison JC, Zyabrev SV (2009) Radiolarian age constraints on Mesotethyan ocean evolution, and their implications for development of the Bangong–Nujiang suture, Tibet. J Geol Soc 166:689–694. doi:10.1144/0016-76492008-128

Belousova E, Griffin WL, O'reilly SY, Fisher N (2002) Igneous zircon: trace element composition as an indicator of source rock type. Contrib Miner Petrol 143:602–622

BouDagher-Fadel MK (2008) Evolution and geological significance of larger benthic foraminifera. In: Developments in palaeontology and stratigraphy, vol 21. Elsevier

Chang CP, Angelier J, Huang CY, Liu CS (2001) Structural evolution and significance of a mélange in a collision belt: the Lichi Mélange and the Taiwan arc–continent collision. Geol Mag 138:633–651. doi:10.1017/S0016756801005970

Chen Y, Zhang K, Li G, Nimaciren ZS, Chen G (2005) Discovery of an uniformity between the Upper Triassic Quehala Group and its underlying rock series in the central segment of the Bangong Co-Nujiang junction zone, Tibet, China (in Chinese with English abstract). Geol Bull China 24:621–624

Chen W, Yang T, Zhang S, Yang Z, Li H, Wu H, Zhang J, Ma Y, Cai F (2012) Paleomagnetic results from the Early Cretaceous Zenong Group volcanic rocks, Cuoqin, Tibet, and their paleogeographic implications. Gondwana Res 22:461–469. doi:10.1016/j.gr.2011.07.019

Chu MF, Chung SL, Song B, Liu D, O'Reilly SY, Pearson NJ, Ji J, Wen D-J (2006) Zircon U–Pb and Hf isotope constraints on

the Mesozoic tectonics and crustal evolution of southern Tibet. Geology 34:745–748
Deng J, Wang Q, Li G, Li C, Wang C (2014) Tethys tectonic evolution and its bearing on the distribution of important mineral deposits in the Sanjiang region, SW China. Gondwana Res 26:419–437. doi:10.1016/j.gr.2013.08.002
Dewey JF, Shackleton RM, Chengfa C, Yiyin S (1988) The tectonic evolution of the Tibetan Plateau. Philos Trans R Soc Lond Ser A Math Phys Sci 327:379–413
Dickinson WR, Gehrels GE (2009) Use of U–Pb ages of detrital zircons to infer maximum depositional ages of strata: a test against a Colorado Plateau Mesozoic database. Earth Planet Sci Lett 288:115–125
Dickinson WR, Suczek CA (1979) Plate tectonics and sandstone compositions. AAPG Bull 63:2164–2182
Dickinson WR, Beard LS, Brakenridge GR, Erjavec JL, Ferguson RC, Inman KF, Knepp RA, Lindberg FA, Ryberg PT (1983) Provenance of North American Phanerozoic sandstones in relation to tectonic setting. Geol Soc Am Bull 94:222–235
Diekmann B, Hofmann J, Henrich R, Fütterer DK, Röhl U, Wei KY (2008) Detrital sediment supply in the southern Okinawa Trough and its relation to sea-level and Kuroshio dynamics during the late Quaternary. Mar Geol 255:83–95. doi:10.1016/j.margeo.2008.08.001
Ding L, Kapp P, Wan X (2005) Paleocene–Eocene record of ophiolite obduction and initial India–Asia collision, south central Tibet. Tectonics 24:1–18
Dong C, Li C, Wan Y, Wang W, Wu Y, Xie H, Liu D (2011) Detrital zircon age model of Ordovician Wenquan quartzite south of Lungmuco-Shuanghu Suture in the Qiangtang area, Tibet: constraint on tectonic affinity and source regions. Sci China Earth Sci 54:1034–1042. doi:10.1007/s11430-010-4166-x
Dong X, Zhang Z, Liu F, He Z, Lin Y (2014) Late Paleozoic intrusive rocks from the southeastern Lhasa terrane, Tibetan Plateau, and their Late Mesozoic metamorphism and tectonic implications. Lithos 198–199:249–262. doi:10.1016/j.lithos.2014.04.001
Dou Y, Yang S, Liu Z, Shi X, Li J, Yu H, Berne S (2012) Sr–Nd isotopic constraints on terrigenous sediment provenances and Kuroshio Current variability in the Okinawa Trough during the late Quaternary. Palaeogeogr Palaeoclimatol Palaeoecol 365–366:38–47. doi:10.1016/j.palaeo.2012.09.003
Fan J, Li C, Xie C, Wang M (2014) Petrology, geochemistry, and geochronology of the Zhonggang ocean island, northern Tibet: implications for the evolution of the Banggongco-Nujiang oceanic arm of the Neo-Tethys. Int Geol Rev 56:1504–1520. doi:10.1080/00206814.2014.947639
Gehrels G, Kapp P, DeCelles P, Pullen A, Blakey R, Weislogel A, Ding L, Guynn J, Martin A, McQuarrie N (2011) Detrital zircon geochronology of pre-Tertiary strata in the Tibetan-Himalayan orogen. Tectonics. doi:10.1029/2011TC002868
Griffin W, Wang X, Jackson S, Pearson N, O'Reilly SY, Xu X, Zhou X (2002) Zircon chemistry and magma mixing, SE China: in situ analysis of Hf isotopes, Tonglu and Pingtan igneous complexes. Lithos 61:237–269
Griffin WL, Belousova EA, Shee SR, Pearson NJ, O'Reilly SY (2004) Archean crustal evolution in the northern Yilgarn Craton: U–Pb and Hf-isotope evidence from detrital zircons. Precambr Res 131:231–282. doi:10.1016/j.precamres.2003.12.011
Guynn JH, Kapp P, Pullen A, Heizler M, Gehrels G, Ding L (2006) Tibetan basement rocks near Amdo reveal "missing" Mesozoic tectonism along the Bangong suture, central Tibet. Geology 34:505–508. doi:10.1130/G22453.1
Guynn J, Kapp P, Gehrels GE, Ding L (2012) U–Pb geochronology of basement rocks in central Tibet and paleogeographic implications. J Asian Earth Sci 43:23–50. doi:10.1016/j.jseaes.2011.09.003
Hao LL, Wang Q, Wyman DA, Ou Q, Dan W, Jiang ZQ, Wu FY, Long JH, Li J (2016) Underplating of basaltic magmas and crustal growth in a continental arc: evidence from Late Mesozoic intermediate–felsic intrusive rocks in southern Qiangtang, central Tibet. Lithos 245:223–242. doi:10.1016/j.lithos.2015.09.015
Harris R, Sawyer R, Audley-Charles M (1998) Collisional melange development: geologic associations of active melange-forming processes with exhumed melange facies in the western Banda orogen, Indonesia. Tectonics 17:458–479. doi:10.1029/97TC03083
Hsü KJ (1974) Mélanges and their distinction from olistostromes. Soc Econ Paleontol Mineral Spec Publ 19:321–333
Hsü KJ, Guitang P, Sengör A (1995) Tectonic evolution of the Tibetan Plateau: a working hypothesis based on the archipelago model of orogenesis. Int Geol Rev 37:473–508
Hu X, Garzanti E, Moore T, Raffi I (2015) Direct stratigraphic dating of India–Asia collision onset at the Selandian (middle Paleocene, 59 ± 1 Ma). Geology 43:859–862. doi:10.1130/g36872.1
Ingersoll RV, Bullard TF, Ford RL, Grimm JP, Pickle JD, Sares SW (1984) The effect of grain size on detrital modes: a test of the Gazzi-Dickinson point-counting method. J Sediment Res 54:103–116. doi:10.1306/212f83b9-2b24-11d7-8648000102c1865d
Jackson SE, Pearson NJ, Griffin WL, Belousova EA (2004) The application of laser ablation-inductively coupled plasma-mass spectrometry to in situ U–Pb zircon geochronology. Chem Geol 211:47–69
Ji WQ, Wu FY, Chung SL, Li JX, Liu CZ (2009) Zircon U–Pb geochronology and Hf isotopic constraints on petrogenesis of the Gangdese batholith, southern Tibet. Chem Geol 262:229–245. doi:10.1016/j.chemgeo.2009.01.020
Kang ZQ, Xu JF, Wang BD, Chen JL (2010) Qushenla Formation volcanic rocks in north Lhasa block: products of Bangong Co-Nujiang Tethy's southward subduction (in Chinese with English abstract). Acta Petrol Sin 26:3106–3116
Kapp P, Yin A, Harrison TM, Ding L (2005) Cretaceous-Tertiary shortening, basin development, and volcanism in central Tibet. Geol Soc Am Bull 117:865–878. doi:10.1130/b25595.1
Kapp P, DeCelles P, Leier A, Fabijanic J, He S, Pullen A, Gehrels G, Ding L (2007a) The Gangdese retroarc thrust belt revealed. GSA Today 17:4
Kapp P, DeCelles PG, Gehrels GE, Heizler M, Ding L (2007b) Geological records of the Lhasa-Qiangtang and Indo-Asian collisions in the Nima area of central Tibet. Geol Soc Am Bull 119:917–933
Kidd WSF et al (1988) Geological mapping of the 1985 Chinese-British Tibetan (Xizang–Qinghai) Plateau Geotraverse route. Phil Trans R Soc Lond A 327(1594). doi:10.1098/rsta.1988.0130
Leier AL, DeCelles PG, Kapp P, Gehrels GE (2007a) Lower Cretaceous strata in the Lhasa terrane, Tibet, with implications for understanding the early tectonic history of the Tibetan Plateau. J Sediment Res 77:809–825
Leier AL, Kapp P, Gehrels GE, DeCelles PG (2007b) Detrital zircon geochronology of Carboniferous-Cretaceous strata in the Lhasa terrane, Southern Tibet. Basin Res 19:361–378. doi:10.1111/j.1365-2117.2007.00330.x
Li G, Sandiford M, Liu X, Xu Z, Wei L, Li H (2014a) Provenance of Late Triassic sediments in central Lhasa terrane, Tibet and its implication. Gondwana Res 25:1680–1689. doi:10.1016/j.gr.2013.06.019
Li JX, Qin KZ, Li GM, Richards JP, Zhao JX, Cao MJ (2014b) Geochronology, geochemistry, and zircon Hf isotopic compositions of Mesozoic intermediate–felsic intrusions in central Tibet: petrogenetic and tectonic implications. Lithos 198–199:77–91. doi:10.1016/j.lithos.2014.03.025
Li GM, Li JX, Zhao JX, Qin KZ, Cao MJ, Evans NJ (2015) Petrogenesis and tectonic setting of Triassic granitoids in the Qiangtang

terrane, central Tibet: evidence from U–Pb ages, petrochemistry and Sr–Nd–Hf isotopes. J Asian Earth Sci 105:443–455. doi:10.1016/j.jseaes.2015.02.017

Liu D, Huang Q, Fan S, Zhang L, Shi R, Ding L (2014) Subduction of the Bangong–Nujiang Ocean: constraints from granites in the Bangong Co area, Tibet. Geol J 49:188–206. doi:10.1002/gj.2510

Liu D, Shi R, Ding L, Huang Q, Zhang X, Yue Y, Zhang L (2015) Zircon U-Pb age and Hf isotopic compositions of Mesozoic granitoids in southern Qiangtang, Tibet: Implications for the subduction of the Bangong–Nujiang Tethyan Ocean. Gondwana Res. doi:10.1016/j.gr.2015.04.007 **(in press)**

Ludwig K (2001) Users manual for Isoplot/Ex rev. 3.23. Berkeley Geochronology Centre Special Publication 1

Nimaciren, Xie YW (2005) Discovery of Middle Triassic strata in the Nagqu area, northern Tibet, China, and its geological implications (in Chinese with English abstract). Geol Bull China 24:1141–1149

Nimaciren, Xie YW, Sha ZL, Peng DP, Qiangbazaxi (2004) 1: 250, 000 geological report of Nagqu County with geological map (in Chinese). Xizang Institute of Geological Survey, China University of Geosciences Press, Lhasa, Wuhan

Pan GT, Mo XX, Hou ZQ, Zhu DC, Wang LQ, Li GM, Zhao ZD, Geng QR, Liao ZL (2006) Spatial-temporal framework of the Gangdese Orogenic Belt and its evolution (in Chinese with English abstract). Acta Petrol Sin 22:521–533

Pan G et al (2012) Tectonic evolution of the Qinghai-Tibet Plateau. J Asian Earth Sci 53:3–14. doi:10.1016/j.jseaes.2011.12.018

Pullen A, Kapp P, Gehrels G, DeCelles P, Brown E, Fabijanic M, Ding L (2008) Gangdese retroarc thrust belt and foreland basin deposits in the Damxung area, southern Tibet. J Asian Earth Sci 33:323–336

Rao X, Skelton PW, Sha J, Cai H, Iba Y (2015) Mid-Cretaceous rudists (Bivalvia: Hippuritida) from the Langshan Formation, Lhasa block, Tibet. Pap Palaeontol 1:401–424. doi:10.1002/spp2.1019

Scherer E, Münker C, Mezger K (2001) Calibration of the lutetium-hafnium clock. Science 293:683–687

Sun G, Hu X, Wang J (2011) Petrologic and provenance analysis of the Zongzhuo Mélange in Baisha area, Gyangze, southern Tibet (in Chinese with English abstract). Acta Geol Sin 85:1343–1351

Van Achterbergh E, Ryan C, Griffin W (2001) GLITTER on-line interactive data reduction for the LA-ICPMS microprobe. Macquarie Research Ltd, Sydney

Wang F, Tang Y (1984) Primary analysis of tectonic environment of the ophiolite in northern Tibet (in Chinese). Himal Geol 2:99–113

Wang X, Yang S, Shi J, Guo L, Shi Y, Lu H, Dong H, Xu J, Kong H, Hu X (1988) Discovery of collision mélange in Longquan, Zhejiang Province and its significance for studying collision orogenic belt in southeastern China (in Chinese with English abstract). J Nanjing Univ (Nat Sci) 24:367–378

Wang B, Wang L, Chen J, Liu H, Yin F, Li X (2015) Petrogenesis of Late Devonian-Early Carboniferous volcanic rocks in northern Tibet: new constraints on the Paleozoic tectonic evolution of the Tethyan Ocean. Gondwana Res. doi:10.1016/j.gr.2015.09.007 **(in press)**

Wang BD, Wang LQ, Chung SL, Chen JL, Yin FG, Liu H, Li XB, Chen LK (2016) Evolution of the Bangong–Nujiang Tethyan ocean: insights from the geochronology and geochemistry of mafic rocks within ophiolites. Lithos 245:18–33

Wu FY, Ji WQ, Liu CZ, Chung SL (2010) Detrital zircon U–Pb and Hf isotopic data from the Xigaze fore-arc basin: constraints on Transhimalayan magmatic evolution in southern Tibet. Chem Geol 271:13–25. doi:10.1016/j.chemgeo.2009.12.007

Xu RH, Schärer U, Allègre CJ (1985) Magmatism and Metamorphism in the Lhasa Block (Tibet): a geochronological study. J Geol 93:41–57. doi:10.2307/30075202

XZBGM (1993) Regional geology of Tibet Autonomous Region (in Chinese). Geological Publishing House, Beijing

Yan M, Zhang D, Fang X, Ren H, Zhang W, Zan J, Song C, Zhang T (2016) Paleomagnetic data bearing on the Mesozoic deformation of the Qiangtang Block: implications for the evolution of the Paleo- and Meso-Tethys. Gondwana Res. doi:10.1016/j.gr.2016.01.012 **(in press)**

Yang TN, Zhang HR, Liu YX, Wang ZL, Song YC, Yang ZS, Tian SH, Xie HQ, Hou KJ (2011) Permo-Triassic arc magmatism in central Tibet: evidence from zircon U–Pb geochronology, Hf isotopes, rare earth elements, and bulk geochemistry. Chem Geol 284:270–282. doi:10.1016/j.chemgeo.2011.03.006

Yin A, Harrison TM (2000) Geologic evolution of the Himalayan-Tibetan orogen. Annu Rev Earth Planet Sci 28:211–280

Yin J, Xu J, Liu C, Li H (1988) The Tibetan Plateau: regional stratigraphic context and previous work. Philos Trans R Soc Lond Ser A 327:5–52

Zhai Q, Jahn B, Wang J, Su L, Mo XX, Wang K, Tang S, Lee H (2013) The Carboniferous ophiolite in the middle of the Qiangtang terrane, Northern Tibet: SHRIMP U–Pb dating, geochemical and Sr–Nd–Hf isotopic characteristics. Lithos 168–169:186–199. doi:10.1016/j.lithos.2013.02.005

Zhang KJ, Xia BD, Wang GM, Li YT, Ye HF (2004) Early Cretaceous stratigraphy, depositional environments, sandstone provenance, and tectonic setting of central Tibet, western China. Geol Soc Am Bull 116:1202–1222. doi:10.1130/b25388.1

Zhang Q, Ding L, Cai F, Xu X, Zhang L, Xu Q, Willems H (2012) Early Cretaceous Gangdese retroarc foreland basin evolution in the Selin Co basin, central Tibet: evidence from sedimentology and detrital zircon geochronology. Geol Soc Lond Spec Publ 353:27–44. doi:10.1144/SP353.3

Zhu DC, Mo XX, Niu Y, Zhao ZD, Wang LQ, Liu YS, Wu FY (2009a) Geochemical investigation of Early Cretaceous igneous rocks along an east–west traverse throughout the central Lhasa Terrane, Tibet. Chemical Geology 268:298–312

Zhu DC, Mo XX, Niu Y, Zhao ZD, Wang LQ, Pan GT, Wu FY (2009b) Zircon U–Pb dating and in situ Hf isotopic analysis of Permian peraluminous granite in the Lhasa terrane, southern Tibet: implications for Permian collisional orogeny and paleogeography. Tectonophysics 469:48–60

Zhu DC, Zhao ZD, Niu Y, Dilek Y, Mo XX (2011a) Lhasa terrane in southern Tibet came from Australia. Geology 39:727–730. doi:10.1130/g31895.1

Zhu DC, Zhao ZD, Niu Y, Mo XX, Chung SL, Hou ZQ, Wang LQ, Wu FY (2011b) The Lhasa Terrane: record of a microcontinent and its histories of drift and growth. Earth Planet Sci Lett 301:241–255. doi:10.1016/j.epsl.2010.11.005

Zhu DC, Zhao ZD, Niu Y, Dilek Y, Hou ZQ, Mo XX (2013) The origin and pre-Cenozoic evolution of the Tibetan Plateau. Gondwana Res 23:1429–1454

Zhu DC, Li S-M, Cawood PA, Wang Q, Zhao ZD, Liu SA, Wang LQ (2016) Assembly of the Lhasa and Qiangtang terranes in central Tibet by divergent double subduction. Lithos 245:7–17. doi:10.1016/j.lithos.2015.06.023